Bulletin of Geophysics and Oceanography Vol. XX, n. X, pp. XXX-XXX; Xxxxx 20xx
DOI 10.4430/bgo00483

An attenuation estimate of seismic signals in the Gulf of Naples (Tyrrhenian Sea)

A. Giordano[1], P. Giordano[2], L. De Luca[1] and L. Giordano[3]

[1] *University of Naples Parthenope, Naples, Italy*
[2] *JMA Wireless Italia Technology Center-Teko Telecom, Castel San Pietro Terme, Bologna, Italy*
[3] *University of Naples Federico II, Naples, Italy*

(Received: 24 July 2024; accepted: 1 November 2024; published online: 28 January 2025)

ABSTRACT The realisation of seismic profiles with the seismic reflection technique for geophysical mapping of deep waters is greatly affected by the attenuation of the amplitude of the seismic signals received during propagation. This type of information is of particular interest to designers of marine information and communication systems. The purpose of this study is to directly detect the present-day attenuation of a single sound impulse in seawater, by considering the interference that is created during the acquisition of the seismic signals. This impulse, produced by the boomer seismic source, appears like a 'slap' generated in seawater, has defined characteristics, and is reproducible with good precision.

Key words: boomer, sparker, signal attenuation, seismic line, seismic reflection.

1. Introduction

The study of acoustic propagation in seawater has been a topic of both theoretical and experimental interest over the last 50 years. From the results obtained, there have been numerous applications: from bathymetric surveys with echo sounders to the search for wrecks with acoustic and ultrasonic sonars and to underwater communication. To these, the fields of Physical Oceanography and Marine Geophysics were added for the study of seabeds and sub-bottoms (stratigraphy).

Claiming to say something new in this field is very difficult. Seismic signals, during propagation, are affected by acoustic, constructive or destructive interference on the amplitudes, due to the presence of the hypothetical Chladni figures (Chladni *et al.*, 1787; Zhu and Hu, 2012; Jia *et al.*, 2015; Kourosh *et al.*, 2017; Tuan *et al.*, 2018).

The objective of this work is to collect experimental data on a specific area and in a specific season and compare them with the data of other experimenters so as to enrich the existing database. In fact, this is what really interests expert designers of marine information and communication systems.

We do not claim to separate the individual causes of attenuation, but rather to highlight, for an impulsive sound emission in the waters of the Gulf of Naples, the attenuation due to the existence of the various causes, in order to obtain practical experimental values directly and easily usable (Dahm *et al.*, 2006; Beranzoli *et al.*, 2009).

For the measurements carried out, both the boomer seismic source (Fig. 1) and the reference hydrophone mod. 8100 Brueel & Kier, having known characteristics (Fig. 2), were used. For the

Fig. 1 - Boomer source in water.

acquisition, areas with a depth greater than 800 m were chosen, in order to ensure that the pulse reflected by the seabed is of negligible amplitude.

The measurements were carried out, as previously mentioned, in the Gulf of Naples, off the island of Capri, along the following lines: Line 22 and Line Passo3, dotted area in the navigation plan (Fig. 3).

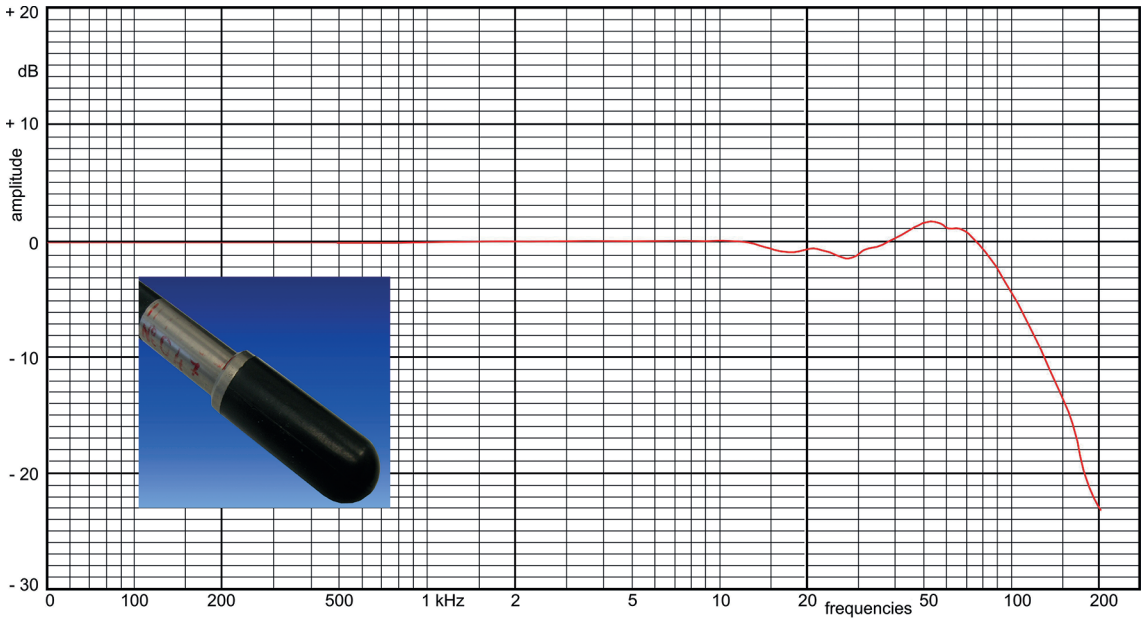

Fig. 2 - Brueel & Kier reference hydrophone.

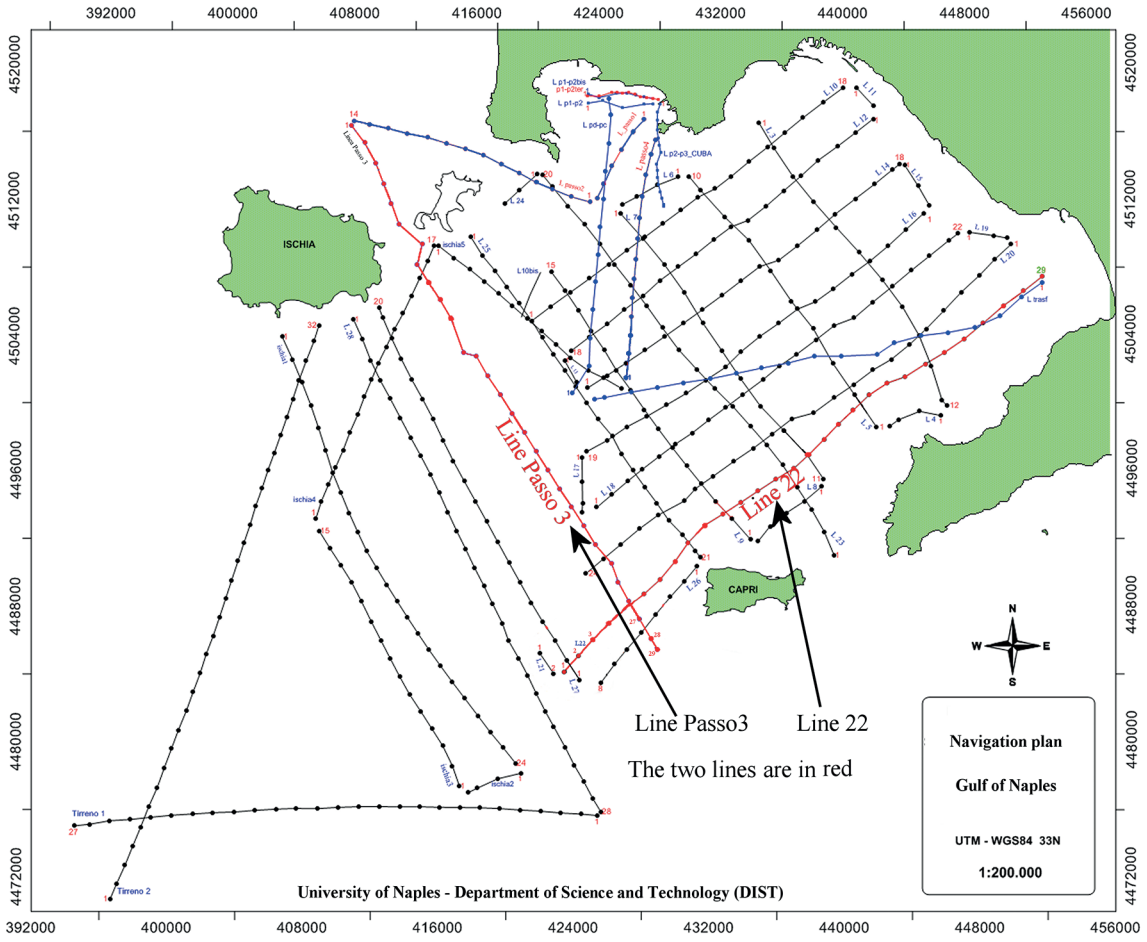

Fig. 3 - Navigation plan: the two lines are highlighted in red.

Many causes influence the attenuation of sound waves during their journey in seawater. In this section, we briefly list these phenomena that have been widely studied from both a theoretical and experimental point of view (Rayleigh, 1945; Urick, 1975; Ziolkowski *et al.*, 1982; Hustedt and Clark, 1999; Reine *et al.*, 2009). The various causes are listed below.

1.1. Divergence of sound waves

If seawater were ideally elastic and homogeneous, the sound waves emitted by an immersed acoustic source, would undergo, during their propagation, half the attenuation for twice the distance travelled by the source (Baccheschi, 2011). This type of attenuation is due to the spherical divergence of the sound rays moving away from the source, just as the light rays emitted by a common incandescent lamp diverge in such a way that the light perceived by the eye decreases with distance. The expression that enables the calculation of the extent of attenuation for spherical divergence, as a function of the length of the path of the acoustic rays, is the following:

$$TL = 20 \log (D) \quad (1)$$

where, *TL* (transmission loss) is expressed in dB and *D* (distance travelled by waves) is expressed in metres.

1.2. Non-adiabatic phenomenon of sound waves

Unfortunately, seawater is neither perfectly elastic nor perfectly homogeneous, so in addition to attenuation due to the divergence of sound rays, there are other causes of a different nature. One of the easily predicted causes of attenuation is due to the loss of acoustic energy by partial absorption by water molecules, which is converted into heat (Hustedt and Clark, 1999). Alternating compression and decompression of sound waves creates transformations with heat dissipation between adjacent layers. The medium heats up and the resulting energy is subtracted from that of the migrating sound wave. This attenuation is also proportional to frequency squared.

1.3. Medium viscosity

The propagation of sound in water is characterised by absorption and diffusion, which, overall, define the attenuation of the acoustic wave (Monna and Dahm, 2009; De Siena *et al.*, 2010; Baccheschi, 2011). Absorption α is due to viscosity and increases with the frequency, *f,* squared of the acoustic signal:

$$\alpha \infty f^2. \tag{2}$$

This means that the different components of the signal spectrum are absorbed differently or, in other words, that propagation modifies the signal spectrum. Diffusion (scattering) is a consequence of the fact that water is not a homogeneous medium but, on the contrary, it is characterised by the presence of microstructures, such as bubbles, plankton, and particulates. The Beer law describes the attenuation of the acoustic signal as a function of the distance from the source and establishes that energy loss is proportional to energy itself, i.e. it defines a law with a decreasing exponential trend to characterise acoustic propagation:

$$\frac{dI}{dD} = -\alpha \cdot I \tag{3}$$

where I is the intensity of the acoustic wave, D is the distance from the source, and $\alpha(f)$ is the attenuation coefficient. This, in addition to the frequency, also depends on the physical properties of the medium, in particular, on viscosity η and density ρ of the medium (Caloi and Spadera, 1959; Scherbaum, 1990; Knauss, 1997). Viscoelasticity is the property of materials that exhibit an intermediate rheological behaviour between that of purely viscous materials and elastic materials. Viscous materials, like water, resist shear flow but strain when a stress is applied. The attenuation of viscous materials, such as water, is due to viscous tangential forces, whose work is carried out at the energy expense of the migrating sound wave (Fig. 4). In theory, attenuation has an exponential trend.

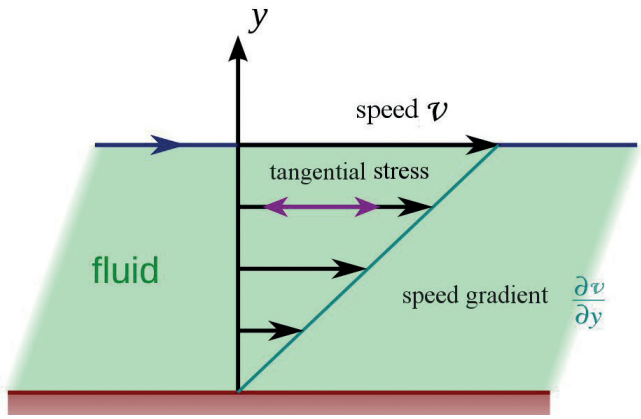

Fig. 4 - Example of viscous friction.

1.4. Suspended materials

The presence of suspended materials in the sea, especially air bubbles in the layers closest to the free air, produces gradual reflections that attenuate and tend to bend the sound rays, (Yuric, 1967).

1.5. Curvature of the sound beams

As depth changes, the presence of temperature, salinity, and pressure gradients produces a change in water density, which in turn produces a change in acoustic impedance *Z* of the water:

$$Z = \rho \cdot v \tag{4}$$

where ρ is the density of the materials and v the speed of sound in the materials. The variation of these parameters creates vertical marine stratification along the water column.

In the Tyrrhenian Sea, where the value of the average sound propagation speed is about 1530 m/s (Wilson, 1960; Stabile *et al.*, 2007), depending on the magnitude of the gradients mentioned above, a sound beam that is initially straight and vertical with respect to the horizontal plane tends to change its inclination by curving (Urick, 1975; De Dominicis Rotondi, 1990; Yilmaz, 2001). The curvature can be downwards or upwards, depending on the change in acoustic impedance *Z* (Corradi *et al.*, 2004; Tsuchiya *et al.*, 2008; Giordano and Giordano, 2012).

In general, the attenuation of an acoustic beam with a certain slope can be either positive or negative, i.e. there can be an increase in signal intensity as the distance from the source increases and vice versa, depending on the gradients mentioned above. Conditions may occur where an inversion of the curvature occurs, with a change in the sign of the acoustic beam.

1.6. Medium crystallisation

The high polarity of water produces a tendency to form pseudo-microcrystals. The result is attenuation due to multiple reflections on the separation surfaces of almost crystalline, acoustically anisotropic structures, which are formed and chaotically destroyed in the mass of the medium. This attenuation, also of exponential trend, increases as frequency increases, giving rise to lateral diffusion of sound beams.

The separation of attenuations due to various causes is usually theoretical and, therefore, the experimental verification of the values of the various components is impossible under real conditions, whereas they have been repeatedly tested under simulated laboratory conditions.

Two series of measurements have been made and they result to be in agreement. More precisely: on Line 22 around Fix 3, with coordinates of 40°31'17.4'' N and 14°06'58.2'' E and a depth of approximately 900 m, and on Line Passo3 around Fix 28, with coordinates of 40°31'24.6'' N and 14°09'27.0'' E and a depth of approximately 1,010 m.

2. Experimental procedure

The seismic sources are systems that generate seismic signals for the study of under seabed stratigraphy. The important feature of seismic sources is the signature. It is different for each individual source. The signature of a seismic source is composed of a main pulse followed by various other oscillations, with periods that depend on the source type, source size, and energy used (Mirabile, 1969; Mirabile *et al.*, 2000). These oscillations are considered annoying as they increase the pulse duration and decrease the vertical resolving power (*VRP*)[1], which can be calculated with the following equation (Widess, 1982):

$$VRP = \left(\frac{v \cdot \tau}{2}\right) \tag{5}$$

where v is the sound speed in water and τ is the duration (ms) of the pulse emitted from the source (acoustic signature).

The boomer is considered a primary source to be used in shallow waters (Tòth *et al.*, 1997; Simpkin, 2005). It enables obtaining seismic profiles with high *VRP* and high penetration in sands, clays, and sediments (Urick, 1979; Verbeek and McGee, 1995; McGee, 2000).

The boomer source consists of a circular coil embedded in an araldite plate, mounted under a catamaran (Fig. 1). Externally to the araldite plate, a metal disk is mounted. It is made of anticorodal aluminium and has a diameter of about 50 cm with a thickness of about 6 mm. It is free to slide axially on a central support (Fig. 5).

This source, featuring a high directivity, also has a maximum resolving power in space-time when the duration of the pulse (signature) approaches the Dirac pulse (Verbeek, 1995).

Traditional sparker-type sources, widely used in CARG (Geological and geothematic cartography) project and the National Research Project in Antartica (PNRA) (Finetti, 1969; De Vita *et al.*, 1979; Jones, 1999; D'Argenio *et al.*, 2004; Corradi *et al.*, 2009; Aiello *et al.*, 2012; Aiello and Marsella, 2016), present a signature (Fig. 6), with a duration of approximately 1.2 ms, that is not suitable for the discrimination of the superficial layers of the seabed. Consequently, such sources present a very low resolution and, in fact, by applying Eq. (5), we obtain *VRP* ~0.9 m. Table 1 shows the comparison between the boomer source and the sparker source. From the values indicated it is clear that the boomer has a short signature at time domain, unlike the sparker source.

The experimental measurements to determine the degree of loss due to the attenuation of seismic signals were carried out according to the scheme shown in Fig. 7. Both the source

[1] The vertical resolving power (*VRP*) is the ability to discriminate, in the vertical plane, two contiguous seismic reflectors.

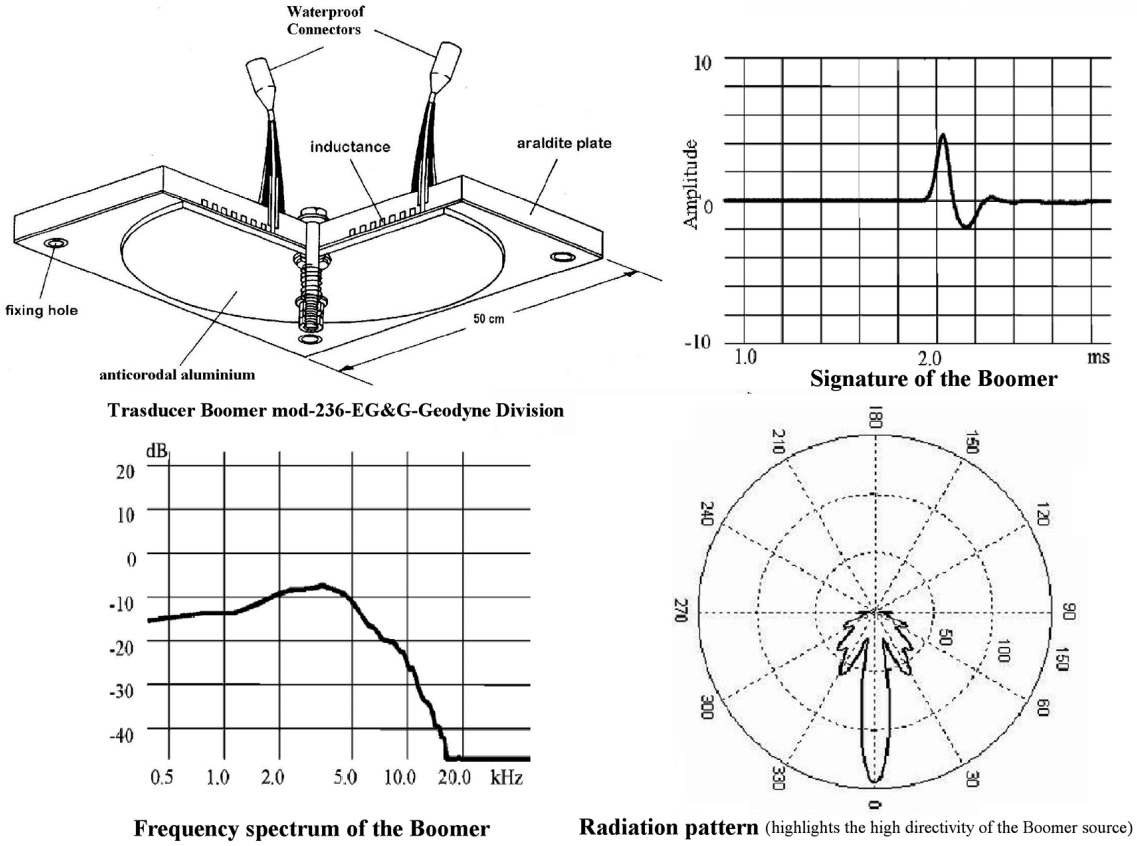

Fig. 5 - Boomer source plate (top left), with its signature and spectral response.

(boomer) and the acoustic receiver (Brueel & Kier reference piezoelectric hydrophone mod. 8100) were placed on two different boats.

When downloading the energy stored by a 4 kV capacitor battery onto the boomer coil, a transient current is generated within the disk. This, being in phase opposition with the current circulating in the coil, creates an impulsive movement of the metal disk, which, in turn, creates a repulsive force, whose effect is a rapid downward thrust of the disk.

The disk, vertically immersed with the araldite plane parallel to the sea surface, creates a hollow bubble followed by the generation of a sound impulse, whose duration τ is about 0.2

Table 1 - Comparison between boomer and sparker sources.

Features of the sources	Boomer	Sparker
Power (J)	200	200
Signature τ (ms)	0.2	1.2
Spectrum (Hz)	100-3000	20-700
Shooting cadence (s)	0.5	0.5
Resolution [*VRP*] (m)	0.15	0.9
Dimensions (m)	1.60×0.9×0.6	2.00×0.3×0.3
Weight (kg)	90	35

ms (Fig. 6). The emission has a directive radiation pattern with an axial symmetry (De Dominicis Rotondi, 1990; Buogo and Cannelli, 1999). Moreover, it has an amplitude spectrum, which practically ends near the 4-5 kHz (Fig. 6). If we assume that our source has the characteristics of a rigid theoretical piston with diameter F (Stepanishen, 1970, 1971), and that the emission takes place on one side of the disk, we obtain radiation pattern $\varphi(\theta)$ of the pressure emitted in the direction of angle θ with the piston axis. This is defined by the following equation:

$$\varphi(\theta) = \frac{J_1\left(\frac{\omega \cdot \Phi \cdot \sin\theta}{v}\right)}{\frac{\omega \cdot \Phi \cdot \sin\theta}{v}} \tag{6}$$

where v is the velocity of the sound in the sea, considering v = 1530 m/s (Stabile *et al.*, 2007), and J_1 is the Bessel function of first species and 1st order.

For a θ = 0° angle, i.e. vertical, the maximum emission is φ (0°) = 1, while for a θ = 90° angle, i.e. for horizontal directions that are parallel to the disk plane, the emission is φ(90°) ≈ 0.8, slightly different from the maximum, at frequencies of approximately 1 kHz.

Note that the other side of the metal disk also emits a sound wave, in the opposite phase to the first. In this way a destructive effect is created. Since this side is very close to the araldite plate, it emits little in water, while, reflection signal due to the araldite plate, contributes to the damping of the impulsive motion of the disk in water.

Clearly, the free disk at the contour, under an impulsive action, can generate all mechanical oscillations at the radial nodal lines and circular nodal lines that go under the name of Chladni figures. The receiver used is a Brueel & Kier reference piezoelectric hydrophone, with well-known characteristics, with a reference sensitivity of -205.7 dB, referring to 1V/µPa ± 3 dB, whose work band reaches a frequency of 100 kHz (Fig. 2). Given the small size of the hydrophone, its isotropy is ensured both in the transverse plane and in the orthogonal plane of the source acoustic axis. The boomer source was immersed at a fixed depth, h_B, of just over 4 m and the receiving hydrophone was placed at a variable depth, h_i, from 0 to 133 m, measured with a calibrated support rope. A weight at the end of the hydrophone should secure the verticality of the supporting rope. The

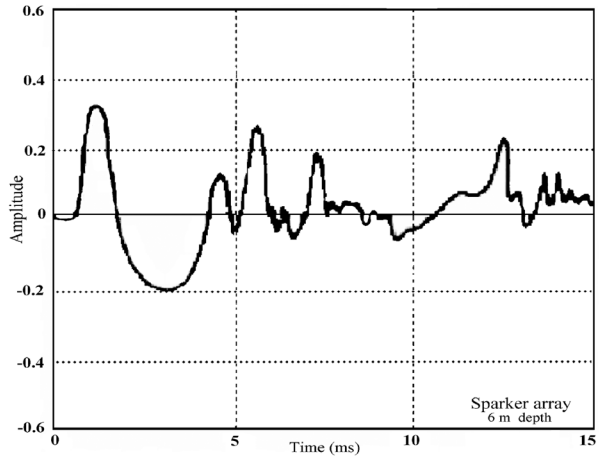

Fig. 6 - Sparker signature.

horizontal distance, *D*, between the source and receiver was fixed to 30 m with a calibrated rope stretched between the two units. It is well known, however, that length measurement errors at sea are remarkable, even if carried out with calibrated ropes (which are subject to variability due to humidity). Influencing the measurement is also the continuous, rather high, movement of the two units, due to the action of wind and sea currents. Finally, given the indeterminacy of the position of the average sea surface, masked by the wave motion, each measure obtained directly should be considered only as guidance. Greater precision in determining distance *D* and height h_B from the transmitter can be obtained by processing the acquired signals with reference to the geometry of Fig. 7, where S indicates the boomer source and R the hydrophone receiver.

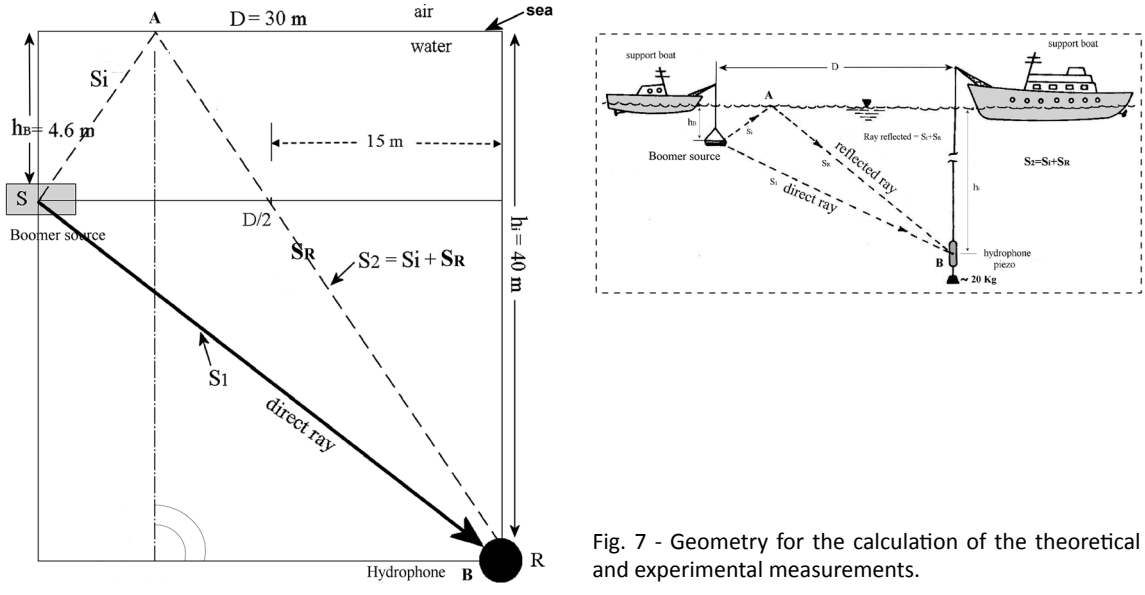

Fig. 7 - Geometry for the calculation of the theoretical and experimental measurements.

3. Acquisition of seismic data

For data acquisition, we used the D-seismic software (Giordano *et al.*, 2002; Corradi *et al.*, 2004), developed at the University of Naples Parthenope (Italy) in the framework of the PNRA. D-seismic is a software that works in a Windows environment, enabling both the acquisition and playback of seismic lines already acquired. The main window is shown in Fig. 8. D-seismic activates the boomer source, generating a zero reference trigger pulse. D-seismic enables to perform real-time analyses of the Fast Fourier Transform frequency spectrum on the seismic signal, both in the acquisition and in the playback phase. This enhances the identification of any correction to be made to the acquisition parameters. The software is able to recondition the seismic signal received by highlighting a good amount of deep layers on the seismic lines, through the application of the time-varied gain tool (Giordano *et al.*, 2015). It is possible to acquire the global positioning system signal, in real time, via a serial connector, in order to georeference both the single signal and the whole seismic line. The analogue-digital conversion of the acquired data takes place through the National Instruments digitising board mod. PCI-MIO 16E, with a sampling frequency up to 200 kHz. The analogue signal, acquired before being subjected to the sampling/digitisation process, was band passed, by appropriate filtering. This was performed by applying a

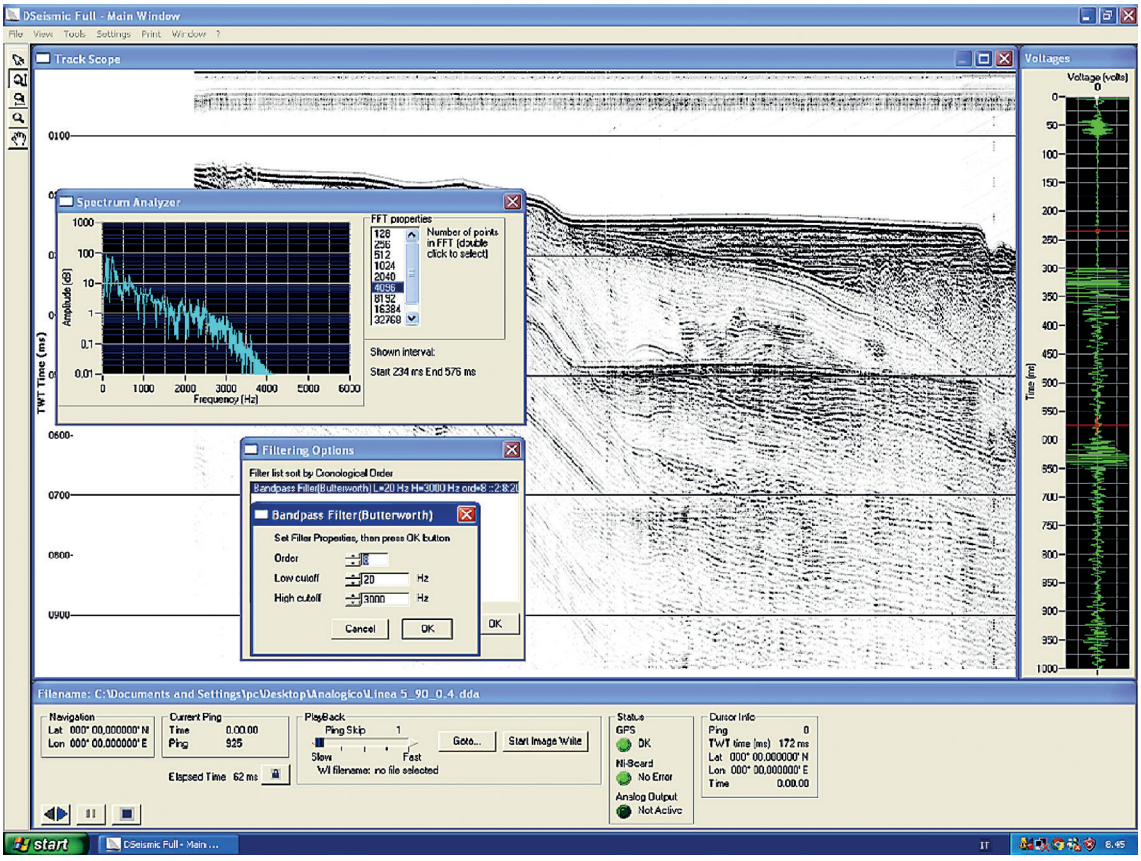

Fig. 8 - The D-seismic main window: with spectral analysis window and applied digital filter window.

filter in the 100-6000 Hz band range and, more precisely, by applying the Krohn-Hite mod. 3700 analogue filter (Kron-Hite Corporation) with high frequency accuracy, in the frequency range from 0.2 to 20 kHz and unity impulse response.

The reflected pulse (compression), from the water/air separation surface of the sea, produces an opposite phase pulse (decompression/ghost reflection), which arrives with a delay, Δt, that is very detectable compared to the primary pulse (see Fig. 10). From the trend of delays Δt detected at various depths h_i of the hydrophone, for a constant distance D, we obtain both depth h_B of the emitter (boomer), and horizontal distance D between the boomer and hydrophone, i.e. h_B = 4.6 m below the average surface of the water (already considered to be about 4 m) and the horizontal distance between the boomer and hydrophone of D = 30 m (already considered to be about 35 m).

For the calculation of the theoretical values of Δt**,** the geometry in Fig. 7 was utilised, with the following relation:

$$\Delta t = T_2 - T_1 \tag{7}$$

where T_2 is the time required by the impulse to travel the distance $S_2 = S_i + S_R$, to reach the receiver, while T_1 is the time required by the direct impulse to reach the hydrophone. If we assume that the propagation velocity, v, in the seawater in the Gulf of Naples (Stabile *et al.*, 2007) is equal to:

$v = S/T \cong 1530$ m/s where $T = S/v$ (8)

where S is the distance travelled.

Consequently, we obtain:

$T_1 = S_1/v \quad T_2 = S_2/v.$ (9)

After fixing the parameters source depth, $h_B = 4.6$ m, source-receiver distance, $D = 30$ m, and varying the depth of the hydrophone from 0 to 130 m, the theoretical curve shows a very good fit with the experimental data.

3.1. Example of theoretical calculation for $h_i = 40$ m

For direct ray path S_1, considering the geometry of Fig. 7, for a fixed value of $h_i = 40$ m and $D = 30$ m, we obtain:

$$S_1 = \sqrt{30^2 + 35.4^2} \cong 46.4 \text{ m.} \quad (10)$$

So, time T_1 to reach the receiver is:

$T_1 = S_1/v \cong 46.4/1530 \cong 0.0309$ s $\cong 30.3$ ms.

For S_2, the entire route is considered:

$S_2 = S_i + S_R$ (11)

with S_i, being the path to point A at the water/air separation surface, while S_R is equal to segment $\overline{AB}$:

$$S_R = \overline{AB} = \sqrt{hi^2 + (\frac{3D}{4})^2} \quad (12)$$

and, when replaced in Eq. (11), the sum becomes:

$$S_2 \cong \sqrt{h_B{}^2 + (\frac{D}{4})^2} + \sqrt{hi^2 + (\frac{3D}{4})^2} \cong S_i + S_R \quad (13)$$

and substituting the values in Eq. (9):

$T_2 = S_2/v \cong 54.7/1530 \cong 0.0365$ s $\cong 35.7$ ms

as a consequence, the difference from Eq. (7) is:

$\Delta t \cong 35.7 - 30.3 \cong 5.4$ ms.

This value agrees with the experimental measures.

The graph in Fig. 9 shows the trend of the experimental measurements of Δ*t* and of the theoretical curve. As we can see, there is a strong correlation between the two curves.

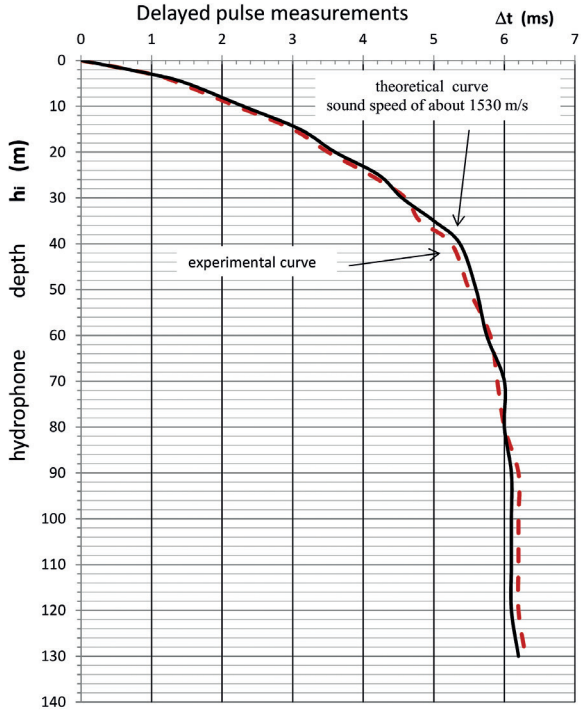

Fig. 9 - Measured experimental values of delay Δ*t* of the reflected impulse, considering a maximum sound speed in the Gulf of Naples, *v* = 1530 m/s (Stabile *et al.*, 2007); parameters: *D* = 30 m and h_B = 4.6.

Fig. 10 shows a generic acquired seismic signal. In it we highlight the portion of the direct signal, to around 30 ms, and the part of the signal reflected from the sea surface. The oscillations of the various portions of the signals are related to the motions of the boomer plate.

The oscillation of the boomer plate, presumably due to the Chladni figures, has higher frequencies than the one of the components contained in the main pulse. Since these oscillation modes are produced simultaneously, interference phenomena occur between them, which are not reproducible from time to time. Furthermore, the directivity diagrams for such frequencies also vary with the movement of the boomer plate due to the effect of the waves.

In fact, the Chladni figures (Zhu and Hu, 2012) with circular nodal lines are determined and constant, while those with radial nodal lines fluctuate due to the effect of the movement of the plate in water. Fig. 10 represents a generic acquired seismic signal. From the reading we note that it includes both the direct impulse and the impulse reflected from the sea surface. The forward pulse is present at approximately 30 ms, using a water velocity of 1530 m/s. The acquisition conditions are: boomer depth h_B = 4.6 m, hydrophone depth h_i = 40 m, and horizontal distance *D* = 30 m.

In moments when various components are in phase, pressure peaks can be compared to those of the direct sound impulse or to those reflected from the sea surface. The oscillations of the reflected Chladni figures have variable directivity even with the instantaneous conformation

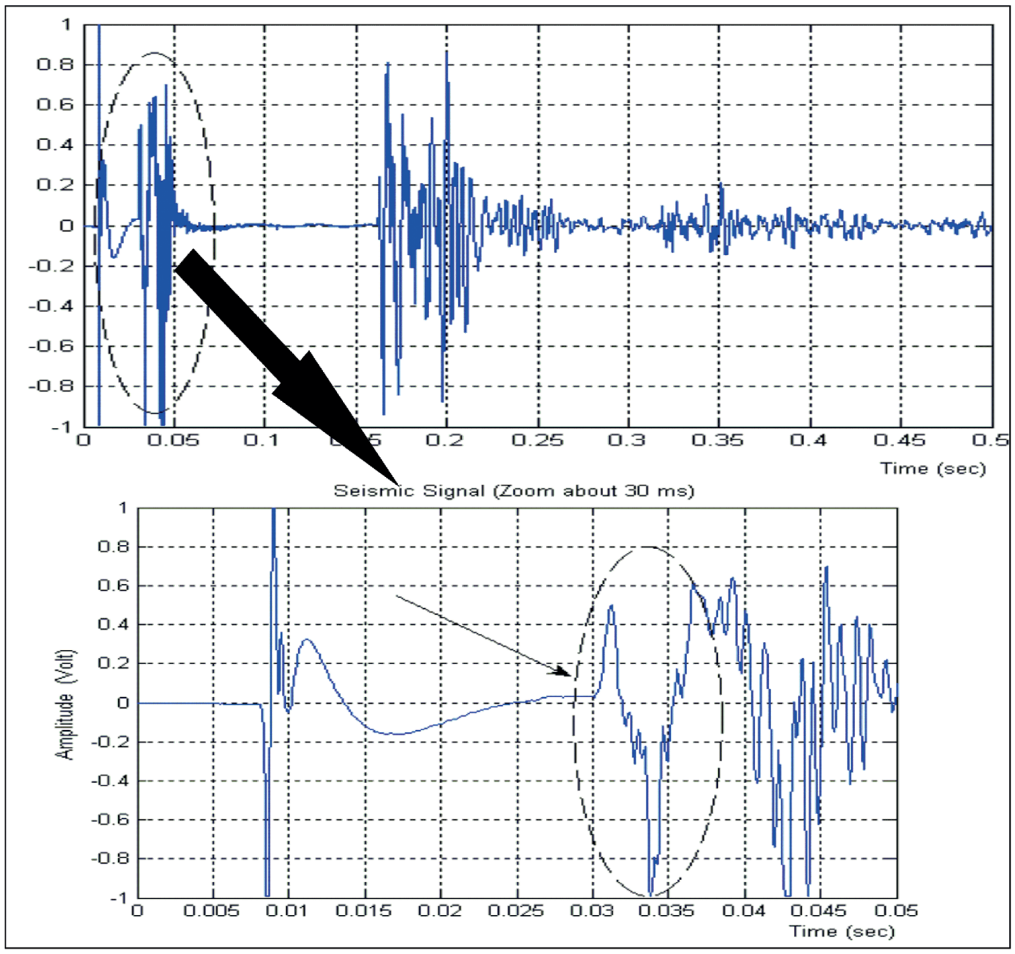

Fig. 10 - The image shows a generic seismic signal acquired during the tests. It can be seen that it includes both the direct pulse and the pulse reflected from the sea surface. Boomer depth h_B = 4.6 m, hydrophone depth h_i = 40 m, and horizontal distance D = 30 m. The direct pulse is present at about 30 ms, using a water velocity of 1530 m/s.

of the sea wave surface. In fact, Fig. 11a shows three signals acquired at a distance of about 10 s one from the other. In them, we note the non-reproducibility of the Chladni figures, while there is good reproducibility of useful impulses.

A further test for the verification of the oscillations that accompany the direct impulse to the reflected one was performed with the boomer plate placed in the air, with adequately reduced energy and receiver directly applied to the plate (Fig. 11b). The data obtained, although of the same nature, appear different from the data acquired at distance in the sea. This difference is due to the fact that, on the disk, the sensor mainly detects oscillations around the measurement point and much fewer oscillations away from the measurement point.

However, in remote measurements, the oscillations of the various portions of the disk are almost equally detected, but regardless of this notable difference, the nature of the oscillations is evident. No electric oscillation was detected during the discharge of the 4 kV load capacitor on the boomer source coil. The measurements at sea were carried out at various boomer-hydrophone horizontal distances, *D*, and various hydrophone depths. Approximately 100 signals were acquired for each point, and they showed a clear difference between the direct impulse

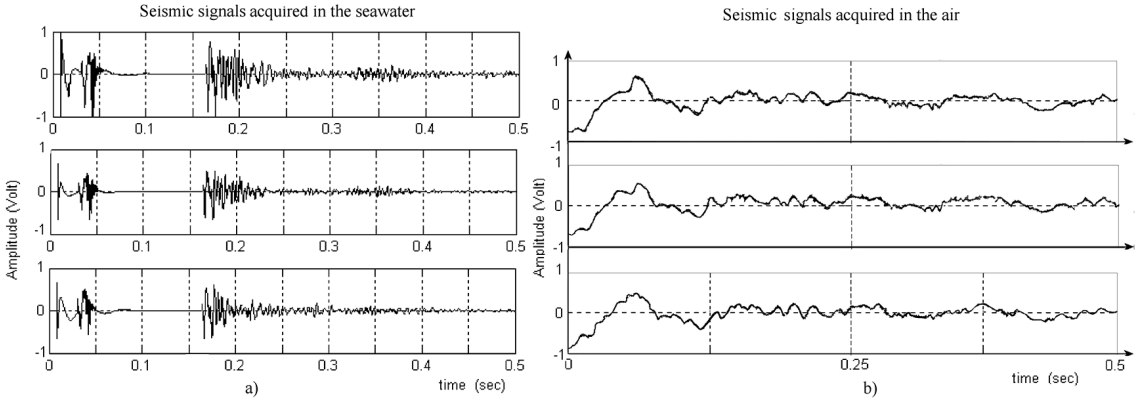

Fig. 11 - The image shows seismic signals acquired at different times, both in the sea (a) and in the air (b). Good reproducibility of useful amplitudes is noted, but there is a non-repeatability of the Chladni figures due to differential effects.

and the pulse reflected by the sea surface, while no clue came from the reflections produced by the hulls of the support boats.

The tests were carried out under good weather conditions, with the sea force never exceeding a sea wave height between 0.1 and 0.3 m. Air temperatures ranged from 17 to 22 °C. In addition, sea temperature data were recorded every three hours up to a depth of 150 m.

4. Sound wave attenuation: experimental values

Horizontal distances *D* of the detection points, from the impulse source and the relative amplitudes of the direct impulse expressed in volts, measured at the output of the hydrophone amplifier, have been reported in the diagram in Fig. 12, where a set of curves dependent on (fixed) depth h_i of the hydrophone were obtained.

Notably, for small depths, h_i, the inclination of the curves is greater than the curve related to the geometrical divergence alone, while it is smaller for high depths, h_i. This causes the curves to intersect. It is noted that the attenuation has a tendency to increase with the increase of horizontal distance *D*. This confirms that sound rays normally tend to bend downwards or upwards according to the temperature along the water column (Urick, 1979; Giordano and Giordano, 2012; Anvari *et al.*, 2017). So, the specific power of the sound pulse decreases compared to the geometric divergence, when distance *D* increases and the depths is low. While it increases at higher depths.

Fig. 13 shows a set of curves, graphically obtained from Fig. 12. These indicate the attenuation of the sound pulse in different directions of a vertical plane passing through the source (boomer). By observing the graphs, we see there is less attenuation of the pulse, compared to rays more inclined to the horizontal plane.

The curves of Fig. 14 represent the quantitative values of all the attenuation causes, obtained on a direct experimental basis, as indicated in section 2. As can be seen, for small inclinations on the horizontal plane, the attenuation in addition to the geometric attenuation is always increasing and positive at any distance.

For higher inclinations, this attenuation is initially positive, reaches a maximum and, then, decreases, becoming and remaining negative.

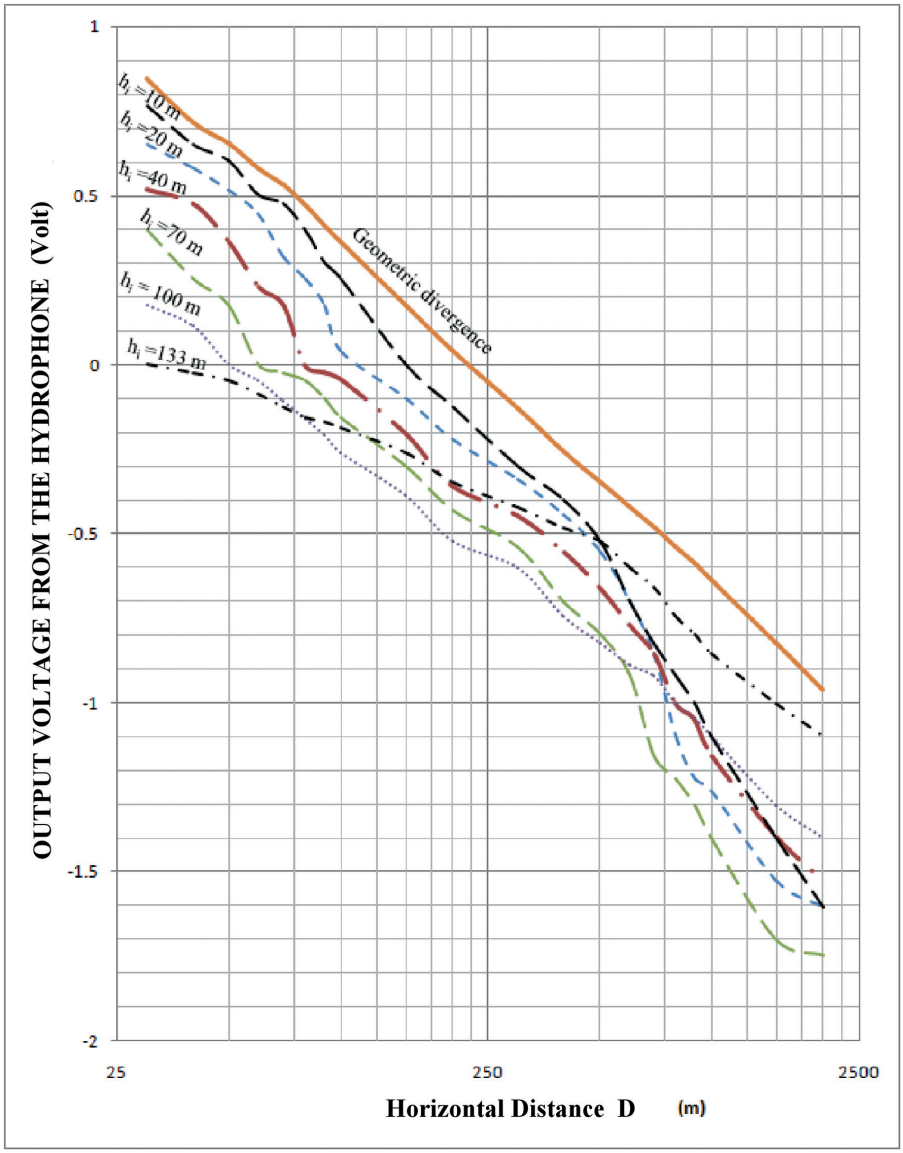

Fig. 12 - Attenuation of the sound pulse emitted by the boomer according to horizontal distance *D* to various h_i depths, see geometry in Fig. 7.

In other words, for inclinations above a certain limit, and at a distance greater than a certain limit, the attenuation of the sound impulse is greater than that of the geometric divergence. This is due to the bending radius phenomenon, which is closely related to the temperature of the water column. Temperature tends to stratify the water column (Stewart, 2008; Tsuchiya *et al.*, 2008).

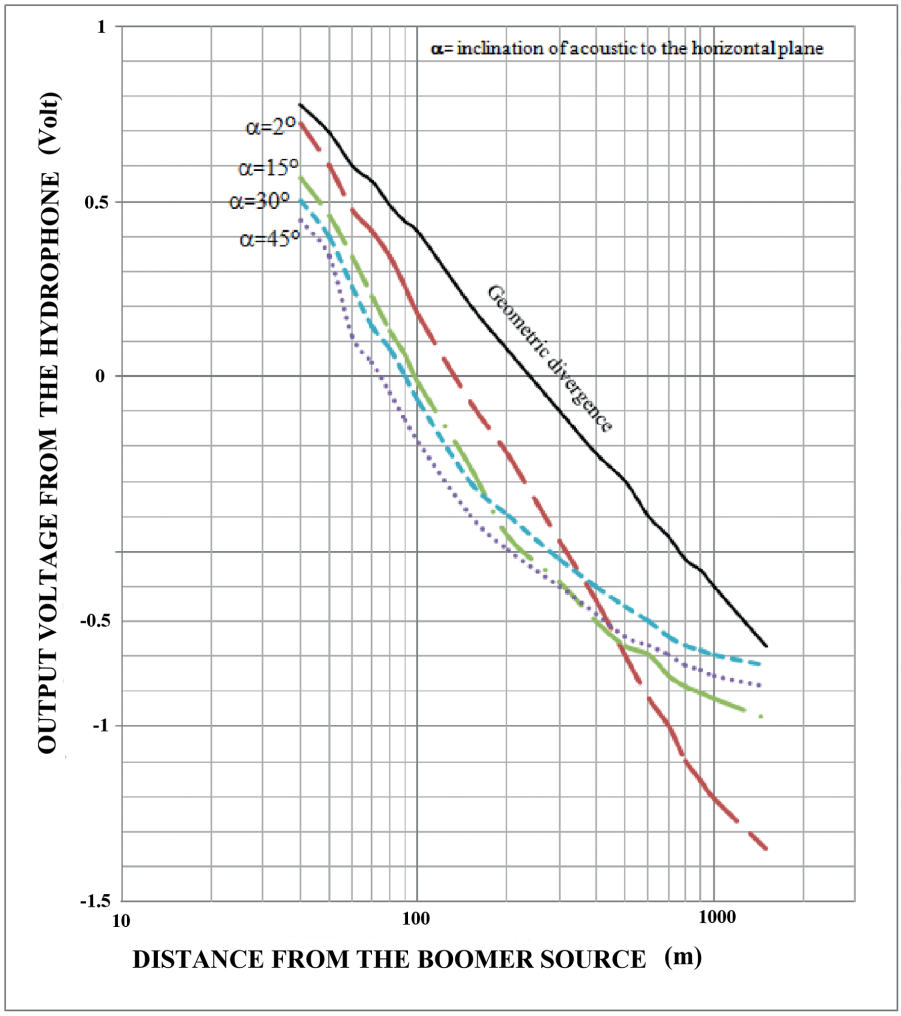

Fig. 13 - Attenuation of the sound pulse in different directions of a vertical plane passing through the generator. α is the angle of the direction of propagation with the horizontal plane.

5. Conclusions

In this work, the effective amplitude attenuation of the seismic signals, due to both the propagation and interferences created on the vibrating metal plate of the boomer (Chladni figure), was experimentally calculated. Numerous practical conclusions, known only qualitatively but confirmed quantitatively in the marine waters of the Tyrrhenian coast, were obtained from the experimental tests. The conclusions reached can be summarised as follows:

- with calm or almost calm seas, the echo emitted from the sea surface originates pulses out of phase by 180°, but with negligible attenuation;
- from 35 to 1000 m, the pulse is measured without detecting significant lengthening of its duration;
- by fixing the hydrophone at a depth of approximately 10 m from the water surface, the signal is no longer perceptible at radial distances greater than 500 m;
- by fixing the hydrophone at a depth greater than 70 m and for radial distances greater

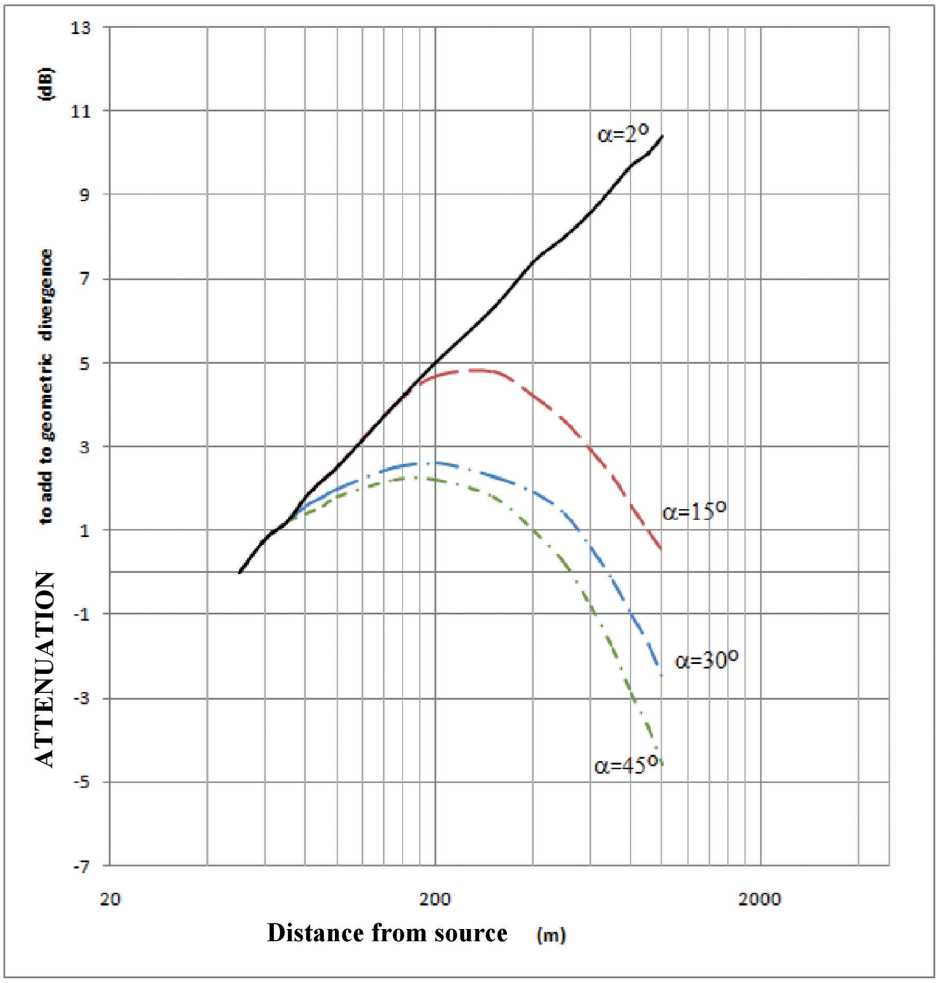

Fig. 14 - Further attenuation beyond the geometric divergence. Attenuation due to the variation of the distance from the sound source and inclination to the horizontal plane, *α*.

than 1000 m, the signal is no longer perceptible because it is masked by the background noise of the receiving system;

- the fundamental (direct) impulse is attenuated much more rapidly than the geometric divergence when the rays have an inclination on the horizontal plane of about 10°. This confirms the curvature of the sound beams as a function of the salinity, pressure, and temperature gradients. Furthermore, the generation of the Chladni figures, caused by the impulsive motion of the boomer plate in water, affects attenuation with interference effects;
- the attenuation due to water viscosity and to the non-perfect adiabatic condition of the sound wave up to 1000-1500 Hz is not appreciable;
- there was no reflection from the hulls of the two boats where both source (boomer) and receiver (hydrophone) were positioned. Signal values were found to be negligible in amplitude;
- during the generation of the sound pulse, no low-frequency electric oscillations were observed in the capacitor discharge circuit on the control coil.

Ultimately, the effective attenuation of a single sound impulse in the sea has been detected. This type of information could be useful for designers of marine information and communication systems, in the field of oceanography, oceanology, and marine geophysics.

Acknowledgments. The authors would like to thank Lorenzo Mirabile of the University of Naples Parthenope, formerly Royal Naval Institute, for his teaching both theory and practice, and for his invaluable help during the marine geophysical surveys.

REFERENCES

Aiello G. and Marsella E.; 2016: *Marine geophysics of the Naples Bay (southern Tyrrhenian Sea, Italy): principles, applications and emerging technologies.* In: Aiello G. (ed), Geophysics, Nova Science Publishers Inc., New York, NY, USA, pp. 61-122.

Aiello G., Giordano L., Marsella E. and Passaro S.; 2012: *Seismic stratigraphy and marine magnetics of the Naples Bay (southern Tyrrhenian Sea, Italy): the onset of new technologies in marine data acquisition, processing and interpretation.* In: Elitok O. (ed), Stratigraphic Analysis of Layered Deposits, Intech Science Publishers, Rijeka, Croatia, pp. 21-60.

Anvari R., Siahsar M.A.N., Gholtash S., Kahoo A.R. and Mohammadi M.; 2017: *Seismic random noise attenuation using Synchrosqueezed Wavelet Transform and Low-Rank Signal Matrix Approximation.* IEEE Trans. Geosci. Remote Sens., 55, 6574-6581, doi: 10.1109/TGRS.2017.2730228.

Baccheschi P.; 2011: *Structure of the southern Tyrrhenian subduction system: insights from seismological analysis of anisotropy and attenuation.* PH.D. Thesis in Geophysical Sciences, XXIII cycle, Alma Mater Studiorum, Università degli Studi di Bologna, Bologna, Italy, pp. I-XVII, doi: 10.6092/unibo/amsdottorato/3597.

Beranzoli L., Favali P., Montuori C., De Santis A., Frugoni F., Calcara M., Iafolla V., Qamili E., Sgroi T., Ciafardini A., Lo Bue N. and Vitale S.; 2009: *Multiparametric seafloor exploration: the Marsili Basin and Volcanic Seamount case (Tyrrhenian Sea, Italy).* In: Proc. 3rd IASME/WSEAS International Conference on Geology and Seismology (GES'09), Cambridge, UK, pp. 153-157.

Buogo S. and Cannelli G.B.; 1999: *Source level and directivity pattern of an underwater pulsed sound generator based on electrical discharge.* Acoust. Lett., 23, 54-59.

Caloi P. and Spadera M.C.; 1959: *Le oscillazioni libere dal golfo di Civitavecchia e l'azione della viscosità cinematica*. Ann. Geophys., 12, 161-177, doi: 10.4401/ag-5646.

Chladni E.F.; 1787: *Entdeckungen* über *die Theorie des Klanges.* Breitkopf und Härtel, Leipzig, Germany, 77 pp., doi: 10.1007/978·3-322·93038-5.

Corradi N., Giordano F. and Giordano R.; 2004: *The application of a very high resolution hardware and software (D-Seismic) system for the loss of seismic data for the study of the Ross Sea sedimentary.* In: Atti Associazione Italiana Oceanologia Limnologia, Genova, Italy, vol. 17, pp. 115-124.

Corradi N., Ferrari M., Giordano F., Giordano R., Ivaldi R. and Sbrana A.; 2009: *SAM source and D-seismic system: the use in Marine Geological Mapping CARG and PNRA Projects.* In: Extended Abstract 27th IAS Meeting of Sedimentologists, Alghero, Italy, pp. 85-90.

D'Argenio B., Aiello G., de Alteriis G., Milia A., Sacchi M., Tonielli R., Angelino A., Budillon F., Chiocci F.L., Conforti A., De Lauro M., Di Martino G., D'Isanto C., Esposito E., Ferraro L., Innangi S., Insinga D., Iorio M., Marsella E., Molisso F., Morra V., Passaro S., Pelosi N., Porfido S., Raspini A., Ruggieri S., Sarnacchiaro G., Terranova C., Vilardo G. and Violante C.; 2004: *Digital elevation model of the Naples Bay and adjacent area (eastern Tyrrhenian Sea, Italy)*. Atlante di Cartografia Geologica, Servizio Geologico d'Italia (APAT), Roma, Italy.

Dahm T., Tilmann F. and Morgan J.P.; 2006: *Seismic broadband ocean-bottom data and noise observed with free-fall stations: experiences from long-term deployments in the north Atlantic and the Tyrrhenian Sea.* Bull. Seismol. Soc. Am., 96, 647-664, doi: 10.1785/0120040064.

De Dominicis Rotondi A.; 1990: *Principi di elettroacustica subacquea.* Elettronica San Giorgio - ELSAG S.p.A., Genova, Italy, Voll. I e II, 414 pp.

De Siena L., Del Pezzo E. and Bianco F.; 2010: *Seismic attenuation imaging of Campi Flegrei: evidence of gas reservoirs, hydrothermal basins, and feeding systems.* J. Geophys. Res., 115, B09312, doi: 10.1029/2009JB006938.

De Vita S., Esposito B. and Mirabile L.; 1979: *Criteri di progetto di sparker a cortina per sismica ad alta risoluzione*. In: Atti Convegno Scientifico Nazionale Progetto Finalizzato Oceanografia e Fondi Marini, CNR, Roma, Italy.

Finetti I.; 1969: *La moderna prospezione sismica digitale per la ricerca di idrocarburi in mare.* Estratto dalla Rivista Italiana del Petrolio, Osservatorio Geofisico Sperimentale, Trieste, Italy, 32 pp.

Giordano A. and Giordano L.; 2012: *Osservazione del comportamento della colonna d'acqua rispetto ai segnali sparker nel mare antartico*. Atti Fond. G. Ronchi, 67, 653-674.

Giordano A., De Luca L., De Luca C., Giordano P. and Giordano L.; 2015: *Controllo del guadagno in ampiezza di segnali sismici a riflessione nel dominio del tempo mediante il filtro TVG (Time Varying Gain).* Atti Fond. G. Ronchi, 70, 215-226.

Giordano F., Giordano R. and Corradi N.; 2002: *D-Seismic: a very flexible low cost hardware/software system for acquisition, real time and post processing of seismic data of Ross Sea (Antartica 2002 expedition)*. In: Proc. Forum ACUSTICUM, Seville, Spain, 7 pp., <www.sea-acustica.es-43.40.Ph.001>.

Hustedt B. and Clark R.A.; 1999: *Source/receiver array directivity effects on marine seismic attenuation measurements.* Geophys. Prospect., 47, 1105-1119.

Jia H., Tang H. and -L. Feng P.X.; 2015: *Multimode SiC trampoline resonators manipulate microspheres to create Chladni figures.* In: Proc. Joint Conference of the IEEE International Frequency Control Symposium & the European Frequency and Time Forum (FCS), Denver, CO, USA, pp. 193-197, doi: 10.1109/FCS.2015.7138821.

Jones E.J.W.; 1999: *Marine Geophysics, 1st ed.* John Wiley & Sons, Chichester, west Sussex, UK, 466 pp.

Knauss J.A.; 1997: *Introduction to Physical Oceanography.* Prentice Hall, Upper Saddle River, NJ, USA, 310 pp.

Kourosh L., Harri W. and Quan Z.; 2017: *Multi-particle acoustic manipulation on a Chladni plate*. In: Proc. International Conference on Manipulation, Automation and Robotics at Small Scales (MARSS), Montreal, QC, Canada, 7 pp., doi: 10.1109/MARSS.2017.8001920.

McGee T.M.; 2000: *High-resolution seismic profiling on water.* Ann. Geophys., 43, 1045-1073, doi: 10.4401/ag-3688.

Mirabile L.; 1969: *Prime esperienze di stratigrafia sottomarina eseguite presso l'Istituto Universitario Navale*. Annali IUN, Vol. XXXVIII, 30 pp.

Mirabile L., De Marinis E. and Frattini M.; 2000: *The Phlegrean Fields beneath the sea: the underwater volcanic district of Naples, Italy.* Boll. Geof. Teor. Appl., 41, 159-186.

Monna S. and Dahm T.; 2009: *Three-dimensional P wave attenuation and velocity upper mantle tomography of the southern Apennines–Calabrian Arc subduction zone*. J. Geophys. Res., 114, B06304, doi: 10.1029/2008JB005677.

Rayleigh J.W.S.; 1945: *The theory of sound, 2nd ed*. Courier Dover Publications, New York, NY, USA, vol. I-II, 1050 pp.

Reine C., van der Baan M. and Clark R.; 2009: *The robustness of seismic attenuation measurements using fixed- and variable-window time-frequency transforms.* Geophys., 74, WA123-WA135.

Scherbaum F.; 1990: *Combined inversion for the three-dimensional Q structure and source parameters using microearthquake spectra.* J. Geophys. Res., 95, 12423-12438.

Simpkin P.G.; 2005: *The Boomer sound source as a tool for shallow water geophysical exploration.* Mar. Geophys. Res., 26, 171-181.

Stabile T.A., Zollo A., Vassallo M. and Iannaccone G.; 2007*: Underwater acoustic channel properties in the Gulf of Naples and their effects on digital data transmission.* Ann. Geophys., 50, 321-328, doi: 10.4401/ag-4427.

Stepanishen P.R.; 1970: *Transient radiation from pistons in an infinite planar baffle*. J. Acoust. Soc. Am., 49, 1629-1638, doi: 10.1121/1.1912541.

Stepanishen P.R.; 1971: *The time dependant force and radiation impedance on a piston in a rigid infinite planar baffle*. J. Acoust. Soc. Am., 49, 3B, doi: 10.1121/1.1912424.

Stewart R.H.; 2008*: Introduction to Physical Oceanography.* Texas A & M University (ed), Department of Oceanography, College Station, TX, USA, 345 pp., doi: 10.1119/1.18716.

Tsuchiya T., Anada T., Endoh N. and Ushio S.; 2008: *Analysis of characteristics of sound propagation in Antarctic Ocean by Parabolic Equation Method.* In: Proc. IEEE Explorer, OCEANS 2008, Quebec City, QC, Canada, pp. 1-5, doi: 10.1109/OCEANS.2008.5152123.

Tòth T., Simpkin P.G., Vida R. and Horvath F.; 1997: *Shallow water single and multichannel seismic profiling in a riverine environment.* The Leading Edge, 16, 1553-1720, doi: 10.1190/1.1437563.

Tuan P.H., Lai Y.H., Wen C.P., Huang K.F. and Chen Y.F.; 2018: *Point-driven modern Chladni figures with symmetry breaking.* Sci. Rep., 8, 10844, doi: 10.1038/s41598-018-29244-6.

Urick R.J.; 1979: *Sound propagation in the sea*. Department of Defense, Office of the Secretary of Defense, Defense Advanced Research Projects Agency (DARPA), Washington, DC, USA, 250 pp.

Verbeek N.H.; 1995: *Aspects of High Resolution Marine Seismics.* Utrecht University, Utrecht, The Netherlands, Gelogica Ultraiectina, 125, 134 pp.

Verbeek N.H. and McGee T.M.; 1995: *Characteristics of high resolution marine reflection profiling sources.* J. Appl. Geophys., 33, 251-260.

Widess M.B.; 1982: *Quantifying resolving power of seismic zero-phase wavelets*. Geophys., 47, 1160-1173, doi: 10.1190/1.1441379.

Wilson W.D.; 1960: *Equation for the speed of sound in the sea water.* J. Acoust. Soc. Am., 32, 1357.

Yilmaz Ö.; 2001: *Seismic Data Analysis: processing, inversion, and interpretation of seismic data.* Society of Exploration Geophysicists, Tulsa, OK, USA, 1028 pp., doi: 10.1190/1.9781560801580.

Urick R.J.; 1975: *Principles of underwater sound.* McGraw-Hill, 384 pp.

Zhu X-b and Hu J-h; 2012: *Experimental investigation of characteristics of Chladni effect.* In: Proc. Symposium Piezoelectricity, Acoustic Waves and Device Applications (SPAWDA), Shanghai, China, pp. 65-68, doi: 10.1109/SPAWDA.2012.6464037.

Ziolkowski A., Parkes G., Hatton L. and Haugland T.; 1982: *The signature of an air gun array: computation from near-field measurements including interactions.* Geophys., 47, 1410-1421.

Corresponding author: Alberto Giordano
Dipartimento di Scienze e Tecnologie, Università degli Studi di Napoli Parthenope
Centro Direzionale, Isola C4, 80133 Napoli
Phone: +39 0815476668; e-mail: alberto.giordano@uniparthenope.it